Thermal Science and Engineering 2024, 7(2), 6914.
https://doi.org/10.24294/tse.v7i2.6914

Article

Numerical heat transfer enhancement in MHD boundary layer flow with Darcy-Forchheimer Bioconvection Nanofluid

Umar Farooq[1,*], Tao Liu[1], Umer Farooq[2]

[1] State Key Laboratory of Fluid Power and Mechatronic Systems, School of Mechanical Engineering, Zhejiang University, Hangzhou 310058, China

[2] College of Mathematical Science, Harbin Engineering University, Harbin city 150001, China

*** Corresponding author:** Umar Farooq, umar_f@zju.edu.cn

CITATION

Farooq U, Liu T, Farooq U. Numerical heat transfer enhancement in MHD boundary layer flow with Darcy-Forchheimer Bioconvection Nanofluid. Thermal Science and Engineering. 2024; 7(2): 6914. https://doi.org/10.24294/tse.v7i2.6914

ARTICLE INFO

Received: 27 February 2024
Accepted: 11 April 2024
Available online: 25 April 2024

Abstract: Scientists have harnessed the diverse capabilities of nanofluids to solve a variety of engineering and scientific problems due to high-temperature predictions. The contribution of nanoparticles is often discussed in thermal devices, chemical reactions, automobile engines, fusion processes, energy results, and many industrial systems based on unique heat transfer results. Examining bioconvection in non-Newtonian nanofluids reveals diverse applications in advanced fields such as biotechnology, biomechanics, microbiology, computational biology, and medicine. This study investigates the enhancement of heat transfer with the impact of magnetic forces on a linearly stretched surface, examining the two-dimensional Darcy-Forchheimer flow of nanofluids based on blood. The research explores the influence of velocity, temperature, concentration, and microorganism profile on fluid flow assumptions. This investigation utilizes blood as the primary fluid for nanofluids, introducing nanoparticles like zinc oxide (ZnO) and titanium dioxide (TiO_2). The study aims to explore their interactions and potential applications in the field of biomedicine. In order to streamline the complex scheme of partial differential equations (PDEs), boundary layer assumptions are employed. Through appropriate transformations, the governing partial differential equations (PDEs) and their associated boundary conditions are transformed into a dimensionless representation. By employing a local non-similarity technique with a second-degree truncation and utilizing MATLAB's built-in finite difference code (bvp4c), the modified model's outcomes are obtained. Once the calculated results and published results are satisfactorily aligned, graphical representations are used to illustrate and analyze how changing variables affect the fluid flow characteristics problems under consideration. In order to visualize the numerical variations of the drag coefficient and the Nusselt number, tables have been specially designed. Velocity profile of ZnO-blood and TiO_2-blood decreases for increasing values of M, λ, and F_r, while temperature profile increases for increasing values of M, λ, and Ec. Concentration profile decreases for increasing values of S_c, and microorganism profile increases for increasing values of Pe. For rising values of M, λ and F_r the drag coefficient increases and the Nusselt number decreases for rising values of M, λ, Ec and Q. The model introduces a novel approach by conducting a non-similar analysis of the Darchy-Forchheimer bioconvection flow of a two-dimensional blood-based nanofluid in the presence of a magnetic field.

Keywords: Bioconvection; MHD; Darcy-Forchheimer; non-similar modeling, bvp4c

1. Introduction

Nanofluids have a range of applications in engineering and biomedicine, including increasing the heat conductivity of fundamental fluids like ethylene glycol, water, kerosene, and others. These applications span the manufacturing industries, treatment for cancer, and conditioning. Buongiorno and Hu [1] conducted research on the enhancement of nanofluid heat transfer for nuclear reactor applications. Buongiorno [2] conducted an extensive study that explored convective transport in nanofluids. The impact of nanofluids thermophysical characteristics on convective heat transfer was explored by Daungthongsuk and Wongwises [3]. Khan and Ali [4] investigated that the non-Newtonian behavior of power-law fluids and wall sliding conditions influences thermal and flow properties such as temperature distribution and viscous heating effects. Ali et al. [5] used a numerical solution based on the Carreau model to critically analyze the flow of a generalized Newtonian fluid over a nonlinearly stretched curved surface. Their research focused on understanding fluid behavior under different shear rates, as well as the effect of surface curvature on flow properties. Mehmood et al. [6] studied the complicated dynamics of these nanotube fluids, especially the effect of activation energy on quaternary autocatalytic exothermic and endothermic chemical processes.

The focus of the field of magneto-hydrodynamics (MHD) is the study of the intricate interaction between magnets and electrically conducting fluids. Due to its extensive practical applications in the chemical and mechanical sectors, this field of study has garnered significant interest. The analysis of MHD's impact on heat transfer and fluid flow over surfaces that are stretched linearly or nonlinearly has received a lot of attention. A comprehensive review conducted by Kandasamy et al. [7] encompassed various investigations that inspected the effect of magnetic fields and various hydrodynamic and thermal boundary conditions on fluid flow across a stretched sheet. Crane [8] published the first analytical solution for the flow of an incompressible viscous liquid over an expanding sheet. Yazdi et al. [9] focused on studying the Magnetohydrodynamic flow and heat transmission through a non-linear porous stretched sheet while considering chemical changes and partial slip. Farooq et al. [10] investigated the MHD flow of a Casson nanofluid with nanoparticles over an extending sheet. Abouasbe et al. [11] investigate the idea of soft solutions in the context of time-fractional Navier-Stokes equations, accounting for the impact of MHD effects. This study investigates the complicated dynamics of MHD in fluid systems.

In the past few decades, substantial advancements have been achieved in the investigation of boundary layer flow and thermal expansion over a extending sheet. This is particularly noteworthy because the findings have numerous practical applications in various industries and technological fields. Several examples include the refrigeration of an unending metal plate within a freezing vessel, the boundary layer along the material conveyor, the flow of liquid film during condensation procedures, cable rolling, paper manufacturing, heated rolling, glass manipulation, and the drawing of plastic foil. The focus of Magyari and Keller [12] was on examining how heat moves in a boundary layer flow due to an exponentially continuous stretching panel without any changes in fluid properties, while also exploring the use of magnetohydrodynamic (MHD). The findings of this study have wide-ranging applications in different environmental and industrial systems, including the design of heat transfer mechanisms, catalytic reactors, geothermal systems, and geophysics. These systems typically involve the saturation of porous materials.

Porous medium flow offers numerous benefits across a diverse range of applications, encompassing fermentation, grain storage, reservoir movement, groundwater contamination, petroleum production, fossil fuel systems, energy storage units, nuclear waste disposal, solar panels, oil resources, groundwater sources, and beyond. Although Darcy's theory [13] formed the foundation for numerous investigations on porous media with low porosity and fluid velocities, it had its limitations with highly permeable media and greater transportation. In situations of high flow rates, the conventional Darcy's law did not consider inertial and edge effects. Thus, Darcy's theory was unsuitable for describing the physical conditions of high-porosity media and velocities. Forchheimer [14] suggested adding a squared flow velocity to the Darcy velocity model to overcome this drawback and allow for the investigation of both boundary parameters and inertia. An inclined stretching sheet with an associated magnetic field in a non-Darcy permeable medium was examined by Wang et al. [15].

The movement of motile microorganisms collectively induces bioconvection, which in turn generates macroscopic convective fluid motion due to density gradients. Bioconvection occurs when self-propelled microorganisms swim in a specific direction, causing an increase in the density of the underlying fluid. Hady et al. [16] examined natural convection around a vertically oriented cone immersed in a permeable medium saturated with gyrotactic microorganisms in a non-Darcian nanofluid. Several researchers [17–28] have explored different systems to comprehend the mechanisms governing the directional motion exhibited by various microorganisms. The researchers confirmed that the presence of self-propelled microorganisms in these nanofluids promotes fluid mixing and inhibits the clustering of nanoparticles, resulting in significant fluid motion at a broader scale in their investigation of nanofluids including bacteria.

Meta-intransitive systems can improve the understanding and optimization of hydrodynamics in porous media under Darcy-Forchheimer bioconvection nanofluids. Researchers can better explain and anticipate complex processes by taking into account nontransitive features such as variable nanoparticle interactions and flow dynamics. This understanding is critical for applications in sectors such as environmental engineering and biotechnology, where precise control of fluid flow and particle movement is required. Metaintransitive systems also pose significant challenges and opportunities in decision theory, game theory, and more complex systems. Incorporating intransitive preferences into the decision-making process is critical to conducting effective multicriteria analysis. Meta-intransitive strategies in game theory can lead to complex interaction structures and consequences that influence strategic decision making. Meta-intransitive qualities also provide insights into new phenomena such as autonomy and patterning that shed light on the dynamics of coupled systems.

The upper bound problem in the Darcy–Forchheimer theory of bioconvection nanofluids is a key problem with important implications. Its resolution can improve the theoretical framework and provide a deeper understanding of the behavior of nanofluids in various situations. Researchers can improve the performance and efficiency of nanofluid-based systems by setting the maximum achievable values of important parameters such as fluid velocity, temperature, nanoparticle concentration, and microbial behavior. Solving this problem is critical to advancing scientific knowledge and practical applications in fields such as environmental engineering, medicine, and nanomaterials.

Many real-life scenarios are intrinsically unique, and this article offers a novel perspective. The non-dimensionalization technique, which uses non-similarity transformations, is more physics-based and accountable. Our key goal is to properly handle non-similar phrases resulting from similarity modifications. To the author's knowledge, no earlier academic works have explored bioconvective nanofluid flow across a stretched surface with temperature-dependent viscosity, as indicated by the literature survey. In our future initiatives, we intend to integrate this research with the subject of Mechatronics, concentrating on the creation and improvement of advanced systems. Our primary focus is on biomedical equipment and biomechanics. This multidisciplinary collaboration has enormous potential since it leverages the information created by our research to promote pioneering solutions that promise in healthcare and biotech. Our goal is to help translate theoretical discoveries into real-world uses, making major contributions to technological advances.

With a keen interest in the aforementioned discoveries and their increasing applicability across various industries, such as engineering, biochemical mechanisms, and biological sciences, our objective is to explore the non-similar analysis of MHD boundary layer flow involving Darcy-Forchheimer convection nanofluids. Specifically, we are concentrating on a flow consisting predominantly of two different nanoparticles, namely ZnO and TiO_2, combined with blood as the base fluid. The addition of ZnO and TiO_2 nanoparticles to blood-base fluid results in a complicated interaction between nanoparticles and the biological system. These nanoparticles, which have a wide range of uses, interact differently inside the circulation due to characteristics such as dimension, chemistry of the surface, and biological compatibility. Knowing these interactions is critical for investigating possible biological applications such as medication administration and medical imaging, while taking into account both the benefits and drawbacks of nanoparticle-blood interactions. To account for the influence of the magnetic field, heat generation, and porosity, we have employed the single-phase nanofluid model developed by Tiwari and Das [29]. The control system has been transformed into a non-similar configuration using suitable transformations. To solve the modified equations, we employed the local non-similarity technique (LNS) developed by Sparrow and Yu [30] and the bvp4c package within the MATLAB computational software. As far as our understanding goes, no prior research has been conducted on this subject. A graphical analysis has been employed to comprehensively examine the effects of dimensionless growth factors on velocity, energy, concentration, and microorganism profiles. Additionally, we present a further numerical investigation of skin friction, the local Nusselt number, and microorganism flux using appropriate methods.

2. Problem formulation

Consider the flow of an incompressible MHD nanofluid in a steady two-dimensional boundary layer containing nanoparticles of titanium dioxide (TiO_2) and zinc oxide (ZnO) disseminated in the base liquid (blood) over a linearly stretched surface with Darcy-Forchheimer bioconvection nanofluids. The Darcy Forchheimer model is employed to explain the porous media. The velocity of the stretched fluid, denoted as U_w, is aligned with the stretched surface, while the ambient velocity remains at zero and the ambient temperature is equivalent to T_∞. $F = \frac{C_b}{\sqrt{k}}$ denoted the porous material inertial coefficient, The variables $T, C,$ and n represent fluid temperature, nanoparticle concentration, and microbe distribution function, respectively. Additionally, the stretched surface is positioned perpendicular to the applied magnetic field B_o. Furthermore, the influence of both porosity and the heat source is considered. **Figure 1** presented illustrates the flow configuration and flow chart of the current investigation. The equations that describe the conservation of mass, momentum, energy, concentration, and microorganism within the boundary layer are also included [10,25,31].

$$\frac{\partial u}{\partial x} + \frac{\partial v}{\partial y} = 0, \tag{1}$$

$$\rho_{nf}\left(u\frac{\partial u}{\partial x} + v\frac{\partial u}{\partial y}\right) = \mu_{nf}\frac{\partial^2 u}{\partial y^2} - \sigma_{nf}B_o^2 u - \frac{\mu_{nf}}{K}u - Fu^2, \tag{2}$$

$$(\rho c_P)_{nf}\left(u\frac{\partial T}{\partial x} + v\frac{\partial T}{\partial y}\right) = k_{nf}\frac{\partial^2 T}{\partial y^2} + \sigma_{nf}(uB_o)^2 + \frac{\mu_{nf}}{K}u^2 + Q_o(T - T_\infty) + Fu^3 \tag{3}$$

$$u\frac{\partial C}{\partial x} + v\frac{\partial C}{\partial y} = D_{nf}\frac{\partial^2 C}{\partial y^2} - K_o(C - C_\infty) + \frac{D_m}{T_m}K_T\frac{\partial^2 T}{\partial y^2}, \tag{4}$$

$$u\frac{\partial n}{\partial x} + v\frac{\partial n}{\partial y} = D_m\frac{\partial^2 n}{\partial y^2} + \frac{bW_c}{(C_w - C_\infty)}\left(\frac{\partial}{\partial y}\left(n\frac{\partial C}{\partial y}\right)\right). \tag{5}$$

Associated boundaries [32] are:

$$\begin{gathered} u = U_w = ax,\ v = v_w = 0,\ T = T_w,\ C = C_w,\ n = n_w,\ at\ y = 0, \\ u \to 0, n \to n_\infty, T \to T_\infty, C \to C_\infty\ as\ y \to \infty. \end{gathered} \tag{6}$$

Here, Equation (1) represents the continuity equation based on the law of conservation of mass; Equation (2) is the momentum equation based on Newton's second law of motion; Equation (3) is the energy equation based on the first law of thermodynamics; Equation (4) is the concentration equation or advection-diffusion equation based on the law of conservation of mass for the scalar quantity; and Equation (5) is the microorganisms equation, which is based on the law of conservation of mass for microorganisms, random motility, and chemotaxis. The associated boundary conditions at the wall surface and far away from the wall are given in Equation (6).

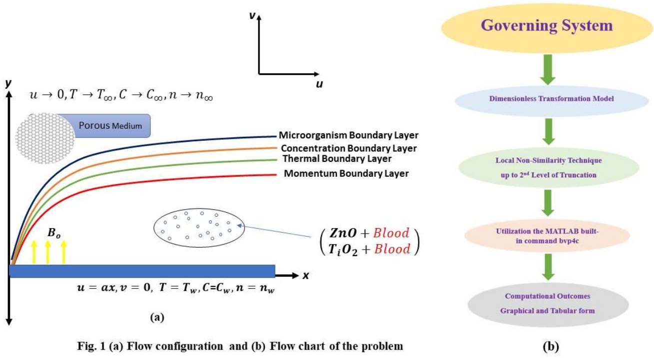

Figure 1. (a) Flow configuration and **(b)** Flow chart of the problem.

Introducing $\xi(x)$ and $\eta(x, y)$ as new terms to create a non-similar flow.

$$\xi=\frac{x}{l},\ \eta=\sqrt{\frac{c}{\upsilon_f}}y, u=cx\frac{\partial f(\xi,\eta)}{\partial\eta},\ v=-\sqrt{\upsilon_f c}\left(\frac{\partial f(\xi,\eta)}{\partial\xi}\xi+f(\xi,\eta)\right),$$
$$\theta(\xi,\eta)=\frac{T-T_\infty}{T_w-T_\infty},\qquad \varphi(\xi,\eta)=\frac{C-C_\infty}{C_w-C_\infty},\qquad \chi(\xi,\eta)=\frac{\mathrm{n}-n_\infty}{n_w-n_\infty} \tag{7}$$

Utilizing Equation (7), Equation (1) is perfectly satisfied given the above transformations, while Equations (2)– (5) become:

$$\frac{\mu_{nf}}{\mu_f}\frac{\partial^3 f}{\partial\eta^3}-\frac{\sigma_{nf}}{\sigma_f}M\frac{\partial f}{\partial\eta}-\frac{\mu_{nf}}{\mu_f}\lambda\frac{\partial f}{\partial\eta}-\left(\frac{\partial f}{\partial\eta}\right)^2\left(\frac{\rho_{nf}}{\rho_f}+F_r\right)+\frac{\rho_{nf}}{\rho_f}f\frac{\partial^2 f}{\partial\eta^2}$$
$$=\xi\frac{\rho_{nf}}{\rho_f}\left(\frac{\partial f}{\partial\eta}\frac{\partial^2 f}{\partial\xi\partial\eta}-\frac{\partial f}{\partial\xi}\frac{\partial^2 f}{\partial\eta^2}\right), \tag{8}$$

$$\frac{k_{nf}}{k_f}\frac{\partial^2\theta}{\partial\eta^2}+PrEc\xi^2\left(\frac{\partial f}{\partial\eta}\right)^2\left(\frac{\sigma_{nf}}{\sigma_f}M+\frac{\mu_{nf}}{\mu_f}\lambda\right)+Pr\left(Q\theta+\frac{(\rho C_p)_{nf}}{(\rho C_p)_f}f\frac{\partial\theta}{\partial\eta}\right)$$
$$+\frac{(\rho C_p)_f}{(\rho C_p)_{nf}}F_r Ec\xi^3\left(\frac{\partial f}{\partial\eta}\right)^3=Pr\xi\frac{(\rho C_p)_{nf}}{(\rho C_p)_f}\left(\frac{\partial f}{\partial\eta}\frac{\partial\theta}{\partial\xi}-\frac{\partial f}{\partial\xi}\frac{\partial\theta}{\partial\eta}\right), \tag{9}$$

$$\frac{D_{nf}}{D_f}\frac{\partial^2\varphi}{\partial\eta^2}+S_c\left(f\frac{\partial\varphi}{\partial\eta}-K_r\varphi+S_r\frac{\partial^2\theta}{\partial\eta^2}\right)=\xi S_c\left(\frac{\partial f}{\partial\eta}\frac{\partial\varphi}{\partial\xi}-\frac{\partial f}{\partial\xi}\frac{\partial\varphi}{\partial\eta}\right), \tag{10}$$

$$\frac{\partial^2\chi}{\partial\eta^2}+Pe\left(\frac{\partial^2\varphi}{\partial\eta^2}(\chi+\delta_1)+\frac{\partial\chi}{\partial\eta}\frac{\partial\varphi}{\partial\eta}\right)+fLe\frac{\partial\chi}{\partial\eta}=\xi Le\left(\frac{\partial f}{\partial\eta}\frac{\partial\chi}{\partial\xi}-\frac{\partial f}{\partial\xi}\frac{\partial\chi}{\partial\eta}\right). \tag{11}$$

The associated non-similar boundaries are as follows:

$$\frac{\partial f}{\partial\eta}(\xi,0)=1, f(\xi,0)+\xi\frac{\partial f}{\partial\xi}(\xi,0)=0, \theta(\xi,0)=1, \varphi(\xi,0)=1,\ \chi(\xi,0)=1,$$
$$\text{at } \eta=0,$$
$$\frac{\partial f}{\partial\eta}(\xi,\infty)\to 0, \chi(\xi,\infty)\to 0, \theta(\xi,\infty)\to 0, \varphi(\xi,\infty)\to 0, \text{as } \eta\to\infty. \tag{12}$$

In above equations $M, F_r, \lambda, Pr, Ec, Q, S_c, K_r, S_r, Pe, \delta_1$, $Le, f, \theta, \varphi,$ and χ represents the magnetic field parameter, Forchheimer number, Porosity parameter, Prandlt number, Eckert number, Heat source, Schmidt number, chemical response parameter, Soret number, Peclet number, microorganism difference parameter, Lewis number, dimensionless stream function, temperature, concentration, and gyrotactic microorganism respectively.

Therefore, the following parameters are defined:

$$\boldsymbol{M}=\frac{\boldsymbol{\sigma_f B_0^2}}{\boldsymbol{c\rho_f}}\qquad \boldsymbol{Q}=\frac{\boldsymbol{Q_0}}{\boldsymbol{c(\rho C_P)_f}}\qquad \boldsymbol{Pe}=\frac{\boldsymbol{bW_c}}{\boldsymbol{D_m}}$$
$$\boldsymbol{F_r}=\frac{\boldsymbol{2Fl}}{\boldsymbol{\rho_f}}\qquad S_c=\frac{\nu_f}{D_f}\qquad \delta_1=\frac{n_\infty}{n_w-n_\infty}$$
$$\boldsymbol{Pr}=\frac{\boldsymbol{\nu_f(\rho C_p)_f}}{\boldsymbol{k_f}}\qquad K_r=\frac{K_o}{a}\qquad Le=\frac{\nu_f}{D_m}$$
$$\boldsymbol{Ec}=\frac{\boldsymbol{c^2 l^2}}{\boldsymbol{(c_p)_f(T_w-T_\infty)}}\qquad S_r=\frac{D_m K_T}{\nu T_m}\frac{(T_w-T_\infty)}{(C_w-C_\infty)}$$

A list of relevant physical quantities can be found in some references [33,34].

$$C_f=\frac{\tau_w}{\rho_f U^2{}_W}, Nu=\frac{xq_w}{k_f(T_w-T_\infty)}, \tau_w=\left(\mu_{nf}\frac{\partial u}{\partial y}\right)_{y=0}, \tag{13}$$

$$q_w = \left(k_{nf}\frac{\partial T}{\partial y}\right)_{y=0}.$$

here C_f, Nu, τ_w, and q_w represents drag coefficient, Nusselt number, surface shear stress, and surface flux.

Dimensionless form of Equation (13) is:

$$C_f(Re_x)^{\frac{1}{2}} = \xi^{-1}\frac{\partial^2 f}{\partial \eta^2}(\xi,0),\ Nu_x(Re_x)^{-\frac{1}{2}} = -\frac{k_{nf}}{k_f}\frac{\partial \theta}{\partial \eta}(\xi,0) \tag{14}$$

3. Methodology for local non-similarity

To investigate the flow of nanofluid over a stretched surface within the boundary layer, we employ the local non-similarity (LNS) method on the dimensionless governing model presented in Equation (8–11) along with the specified boundary conditions (12). In the subsequent section, a thorough, step-by-step elucidation of the LNS method applied to address the given problem will be provided.

The main advantage of LNS is that it doesn't require the resolution of other streamwise points to get non-similar solutions for any streamwise point. Furthermore, the differential equations from which these localized solutions are obtained are ordinary differential equations for computing convenience. Furthermore, this technique allows for a certain degree of precise self-validation. The preparatory process for applying the local non-similarity technique to a particular problem consists of an organized sequence of discrete phases. The actual coordinates x and y are first replaced with the carefully selected transformed coordinates ξ and η. The η coordinate, which includes y, is represented as a pseudo-similarity variable. Its main goal is to reduce the degree to which the answer depends on the streamwise variable x, in the same way that a genuine similarity variable completely eliminates x-dependency. On the other hand, the coordinate ξ depends just on x, and it is frequently used in many problems as a dimensionless representation of x. Because the resultant equations effectively become ordinary differential equations, the computing complexity is decreased by eliminating terms involving $\frac{\partial}{\partial \xi}(.)$. This simplifying also removes the streamwise connection, allowing locally independent solutions to be achieved. While there are computational benefits to this "local similarity" technique, the correctness of the findings may not always be guaranteed.

3.1. First level of truncation

Considering the term ξ are significantly smaller than one at the first truncation level, the right-hand sides of Equations (8–11) become zero. This results in the modified system of equations taking the following form.

$$\frac{\mu_{nf}}{\mu_f}(f''' - \lambda f') - \frac{\sigma_{nf}}{\sigma_f}Mf' + \frac{\rho_{nf}}{\rho_f}(ff'' - (f')^2) - (f')^2 F_r = 0, \tag{15}$$

$$\begin{gathered}\frac{k_{nf}}{k_f}\theta'' + PrEc\xi^2(f')^2\left(\frac{\sigma_{nf}}{\sigma_f}M + \frac{\mu_{nf}}{\mu_f}\lambda\right) + Pr\left(Q\theta + \frac{(\rho C_p)_{nf}}{(\rho C_p)_f}f\theta'\right) \\ + \frac{(\rho C_p)_f}{(\rho C_p)_{nf}}F_r Ec\xi^3(f')^3 = 0,\end{gathered} \tag{16}$$

$$\frac{D_{nf}}{D_f}\varphi'' + S_c(f\varphi' - K_r\varphi + S_r\theta'') = 0, \tag{17}$$

$$\chi'' + Pe(\varphi''(\chi + \delta_1) + \chi'\varphi') + fLe\chi' = 0. \tag{18}$$

With boundary conditions,

$$\begin{gathered} f(\xi,0) = 0, f'(\xi,0) = 1, \theta(\xi,0) = 1, \varphi(\xi,0) = 1, \chi(\xi,0) = 1, \text{at}\ \eta = 0, \\ f'(\xi,\infty) \to 0, \theta(\xi,\infty) \to 0, \varphi(\xi,\infty) \to 0, \chi(\xi,\infty) \to 0, \text{as}\ \eta \to \infty. \end{gathered} \tag{19}$$

3.2. Second level of truncation

To achieve a second-order truncation, it is essential to differentiate Equations (8) – (11) with respect to ξ and introduce additional functions.

In order to achieve the second degree of truncation, the following relations are incorporated:

$$\frac{\partial f}{\partial \xi} = k, \frac{\partial \theta}{\partial \xi} = l, \frac{\partial \varphi}{\partial \xi} = m, \frac{\partial \chi}{\partial \xi} = n \text{ and } \frac{\partial k}{\partial \xi} = \frac{\partial l}{\partial \xi} = \frac{\partial m}{\partial \xi} = \frac{\partial n}{\partial \xi} = 0 \tag{20}$$

Therefore, the modified system of equations at the second degree of iteration is:

$$\frac{\mu_{nf}}{\mu_f}k''' = \frac{\rho_{nf}}{\rho_f}\{3f'k' - 2kf' - fk'' + \xi((k')^2 - kk'')\} + k'\left(\frac{\sigma_{nf}}{\sigma_f}M + \frac{\mu_{nf}}{\mu_f}\lambda\right) \tag{21}$$

$$\begin{aligned} \frac{k_{nf}}{k_f}l'' = &-2PrEc\xi f'\left(\frac{\sigma_{nf}}{\sigma_f}M + \frac{\mu_{nf}}{\mu_f}\lambda\right)(f' + \xi k') \\ &- Pr\frac{(\rho C_p)_{nf}}{(\rho C_p)_f}\{fl' + f'l + \xi(k'l - kl')\} + PrQl' \\ &- \frac{(\rho C_p)_f}{(\rho C_p)_{nf}}3F_rEc(\xi^2(f')^3 + \xi^3(f')^2k'), \end{aligned} \tag{22}$$

$$\begin{aligned} \frac{D_{nf}}{D_f}m'' = &\ Sc(f'm - k\varphi') + \xi Sc(k'm - km') \\ &- Sc(k\varphi' + fm' - Krm + Srl''), \end{aligned} \tag{23}$$

$$n'' = Le(\xi(k'n - kn') - 2k\chi') - Pe(m''(\chi + \delta_1) + \phi''n + n'\phi' + \chi'm'). \tag{24}$$

With associated boundaries,

$$k'(\xi,0) = 0, k(\xi,0) = 0, l(\xi,0) = 0, m(\xi,0) = 0, n(\xi,0) = 0, \text{at}\ \eta = 0, \tag{25}$$

$$k'(\xi,\infty) \to 0, l(\xi,\infty) \to 0, m(\xi,\infty) \to 0, n(\xi,\infty) \to 0, \text{as}\ \eta \to \infty. \tag{26}$$

4. Result and discussion

This section presents a physical discussion using graphs that were generated to inspect the behavior of several dimensionless material variables in relation to velocity, temperature, concentration, and microorganism profiles. Each graph provides a comparison between the two nanofluids ZnO + blood and TiO_2 + blood.

Figure 2 depicts how (M) alters the velocity profile. According to research, larger values of the (M) correlate with lower velocity estimations. Magnetic fields affect fluid flow, causing the velocity profile to fall. The magnetic field creates a Lorentz force in the fluid, which opposes both the magnetic field and the direction of flow. This force stops the fluid from flowing, slows it down, and alters the flow pattern. **Figure 3** depicts the impact of porosity on velocity profiles. By raising the porosity parameter, the porous media becomes more permeable, allowing fluid to flow more easily over it. This raises the fluid's total flow rate. The velocity profile, on the other hand, drops when the flow rate rises because the fluid's internal velocity gradient increases. **Figure 4** shows how changing the Forchheimer number affects the deviation of the velocity distribution. As the Forchheimer number increases, the effect of inertial forces on fluid flow becomes more apparent, resulting in a decrease in fluid velocity. This occurs because the fluid encounters greater resistance when passing through a porous medium due to the combined effects of viscous and inertial drag forces. The higher the Forchheimer number, the stronger the inertial effects, which leads to a decrease in flow acceleration. As a result, the fluid velocity profile is leveled out, demonstrating a more uniform velocity distribution across the flow cross-section. In addition, the boundary layer thickens, which is the region along the wall where the fluid velocity changes from zero (due to the no-slip condition at the wall) to the free-stream velocity. The thickening of the boundary layer is caused by increased drag, which greatly slows down the fluid at the wall, expanding the region over which velocity gradients can be measured.

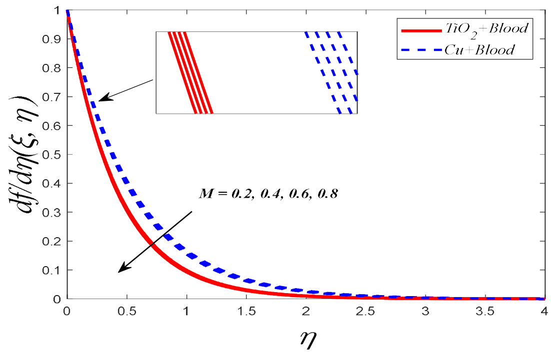

Figure 2. Variation of velocity profile with different values of "M".

If $\xi = 0.5, Q = 1.1, Ec = 1.8, Pr = 21, M = 0.25, \lambda = 1.5, F_r = 1.3, S_c = 2.8, K_r = 0.2, S_r = 0.1, Le = 0.7, \delta_1 = 0.3$.

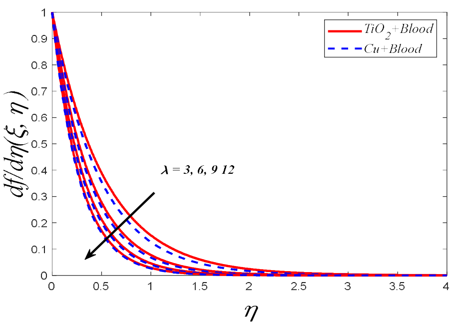

Figure 3. Variation of velocity profile with different values of λ.

If $\xi = 0.5, Q = 1.1, Ec = 1.8, Pr = 21, M = 0.25, \lambda = 1.5, F_r = 1.3, S_c = 2.8, K_r = 0.2, S_r = 0.1, Le = 0.7, \delta_1 = 0.3$.

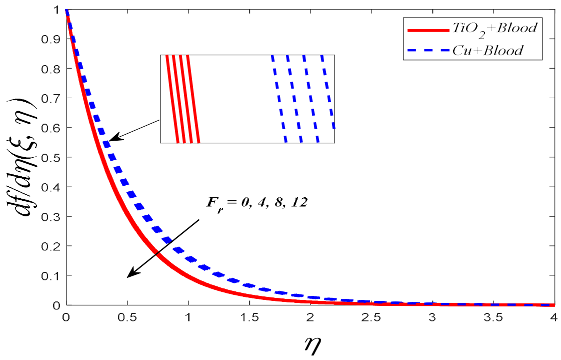

Figure 4. Variation of velocity profile with different values of F_r.

If $\xi = 0.5, Q = 1.1, Ec = 1.8, Pr = 21, M = 0.25, \lambda = 1.5, F_r = 1.3, S_c = 2.8, K_r = 0.2, S_r = 0.1, Le = 0.7, \delta_1 = 0.3$.

Figures 5–7 show that the temperature profile varies depending on the magnetic field parameter (M), porosity parameter (λ) and Eckert number (Ec).

It was found that increasing the magnetic field parameter (M) enhances the magnetic field surrounding the linearly stretched sheet. This stronger magnetic field induces an electric current in the fluid, causing the Lorentz force to resist the fluid's movement. The counteracting Lorentz force leads to an increase in the coefficient of surface friction and the rate of heat transfer on the surface of the sheet. As a result of the increase in thermal energy created by the work done against the Lorentz force, the temperature profile increases. Increasing the porosity parameter (λ) reduces the fluid flow inside the porous medium. This additional obstacle increases the velocity gradient near the linearly stretched layer, causing the fluid to take a more tortuous course. Due to higher frictional heating and viscous energy dissipation, an increase in the velocity gradient leads to an increase in the temperature gradient. As a result, when the porosity parameter increases, the temperature profile also increases. Likewise, an increase in the Eckert number (Ec) indicates that the fluid contains more kinetic energy than thermal energy. This increase in kinetic energy causes greater viscous dissipation, which converts it into thermal energy. As a result, the velocity gradient near the linearly extending sheet increases, resulting in a larger temperature difference. The conversion of kinetic energy to heat increases the temperature profile, demonstrating a clear correlation between the Eckert number and temperature rise. **Figures 8** and **9** show that the Schmidt number (S_c) and Soret number (S_r) vary throughout the concentration profile. As the Schmidt number (S_c) increases, the concentration profiles decrease. The Schmidt number is defined as kinematic viscosity (momentum diffusion coefficient)/mass diffusion coefficient. A larger Schmidt number indicates that mass diffusion is lower than momentum diffusion, meaning that mass (or species) diffuses more slowly than momentum. This reduced mass diffusion rate results in a faster decrease in nanofluid concentration, resulting in a lower concentration profile. From a physical perspective, this means that particles in a nanofluid are less likely to disperse and mix with the surrounding fluid, resulting in steeper concentration gradients and lower overall concentration levels. On the contrary, an increase in the Soret number (S_r) leads to an increase in the concentration profile. The Soret effect, or thermal diffusion, occurs when a temperature gradient causes mass transfer. A higher Soret number indicates that thermal diffusion is more significant than mass diffusion. This means that temperature gradients play a large role in mass transport, causing species to migrate more efficiently from regions of higher temperature to regions of lower temperature. This thermal diffusion effect increases the nanofluid concentration, providing an additional mechanism for mass movement beyond simple mass diffusion. As a result, the concentration profile shifts, revealing greater species concentrations in locations exposed to the temperature gradient. **Figures 10** and **11** depict the dispersion of microbial profiles for different Peclet numbers (Pe) and Lewis numbers. As the Peclet number (Pe) increases, the advection of microorganisms dominates over diffusion. The Peclet number is the ratio of the rates of advective and diffusive transport. A higher Peclet number indicates that the fluid flow is effectively transporting microorganisms down the stretched sheet. This improved advective transport means that microorganisms are carried further from their original position by the fluid flow, resulting in a higher profile of microorganisms in the downstream area. In physical terms, this means that microbes are influenced more by volumetric fluid movement than by random diffusion of molecules, resulting in greater concentrations of bacteria downstream. Conversely, increasing the Lewis number (Le) makes the thermal conductivity coefficient more important than the mass diffusivity coefficient. The Lewis number is calculated as the ratio of the thermal conductivity coefficient to the mass diffusion coefficient. A higher Lewis number indicates that heat travels through the nanofluid faster than microorganisms. As a result, the nanofluid thermally diffuses faster than microorganisms. Thermal diffusion, which is more efficient, affects the temperature distribution within the liquid but does not contribute to the mobility of microbes. As a result, the concentration of microorganisms drops, resulting in a lower microbial profile. This suggests that when Lewis numbers increase, the ability of microbes to spread by diffusion decreases due to the suppressive effect of heat diffusion.

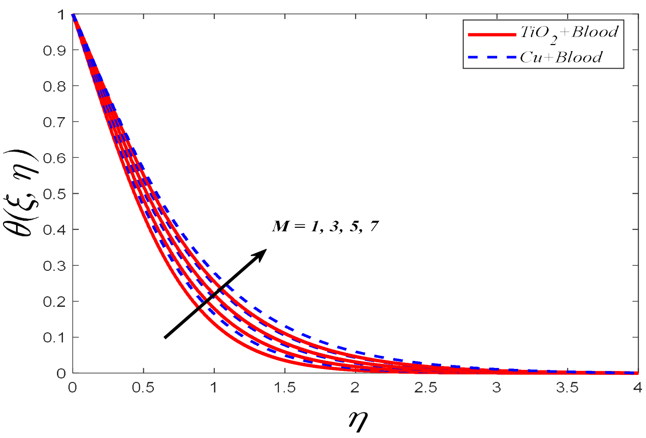

Figure 5. Variation of temperature profile with different values of "M".

If $\xi = 0.5, Q = 1.1, Ec = 1.8, Pr = 21, M = 0.25, \lambda = 1.5, F_r = 1.3, S_c = 2.8, K_r = 0.2, S_r = 0.1, Le = 0.7, \delta_1 = 0.3$.

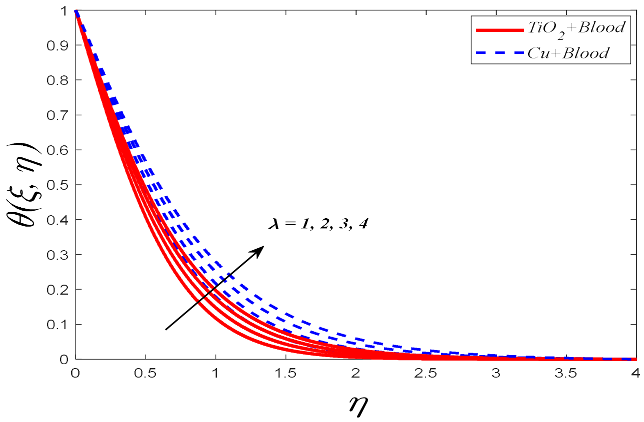

Figure 6. Variation of temperature profile with different values of "λ".

If $\xi = 0.5, Q = 1.1, Ec = 1.8, Pr = 21, M = 0.25, \lambda = 1.5, F_r = 1.3, S_c = 2.8, K_r = 0.2, S_r = 0.1, Le = 0.7, \delta_1 = 0.3$.

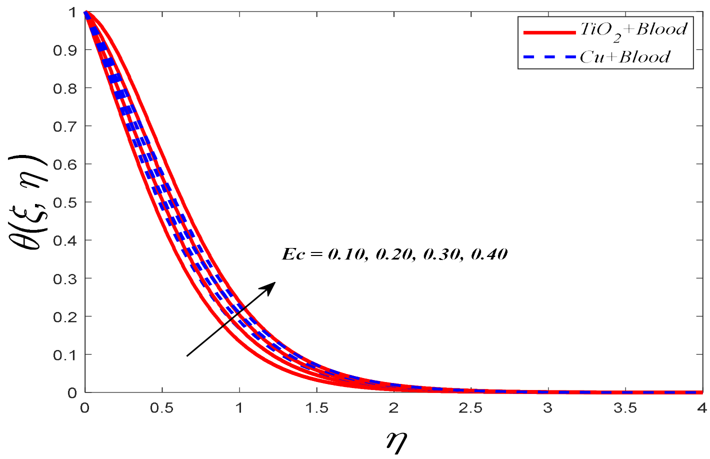

Figure 7. Variation of temperature profile with different values of "Ec".

If $\xi = 0.5, Q = 1.1, Ec = 1.8, Pr = 21, M = 0.25, \lambda = 1.5, F_r = 1.3, S_c = 2.8, K_r = 0.2, S_r = 0.1, Le = 0.7, \delta_1 = 0.3$.

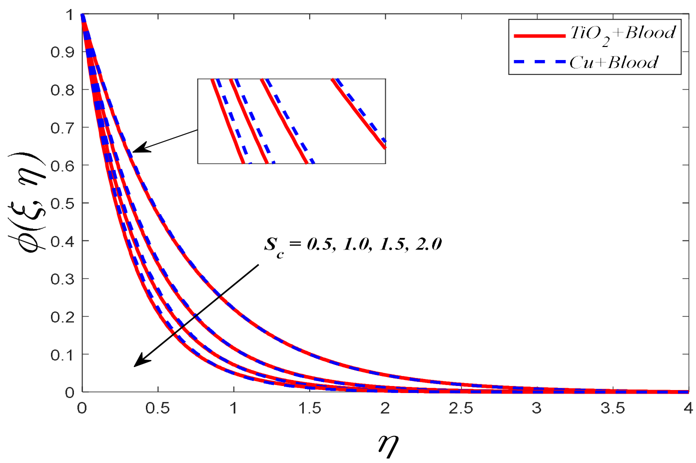

Figure 8. Variation of concentration profile with different values of "S_c".

If $\xi = 0.5, Q = 1.1, Ec = 1.8, Pr = 21, M = 0.25, \lambda = 1.5, F_r = 1.3, S_c = 2.8, K_r = 0.2, S_r = 0.1, Le = 0.7, \delta_1 = 0.3$.

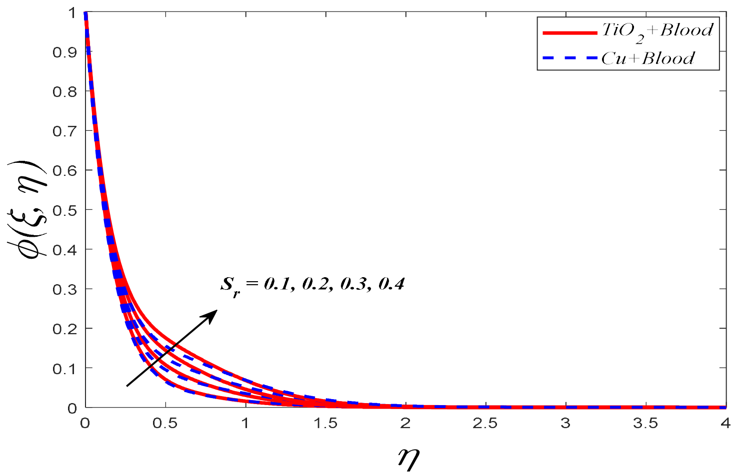

Figure 9. Variation of concentration profile with different values of "S_r".

If $\xi = 0.5, Q = 1.1, Ec = 1.8, Pr = 21, M = 0.25, \lambda = 1.5, F_r = 1.3, S_c = 2.8, K_r = 0.2, S_r = 0.1, Le = 0.7, \delta_1 = 0.3$.

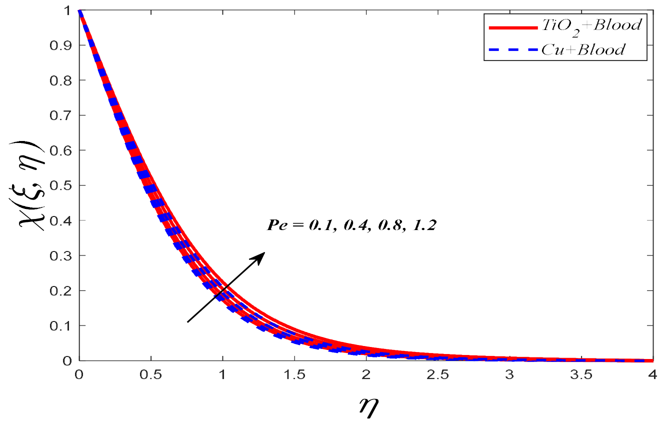

Figure 10. Variation of microorganism profile with different values of "Pe".

If $\xi = 0.5, Q = 1.1, Ec = 1.8, Pr = 21, M = 0.25, \lambda = 1.5, F_r = 1.3, S_c = 2.8, K_r = 0.2, S_r = 0.1, Le = 0.7, \delta_1 = 0.3$.

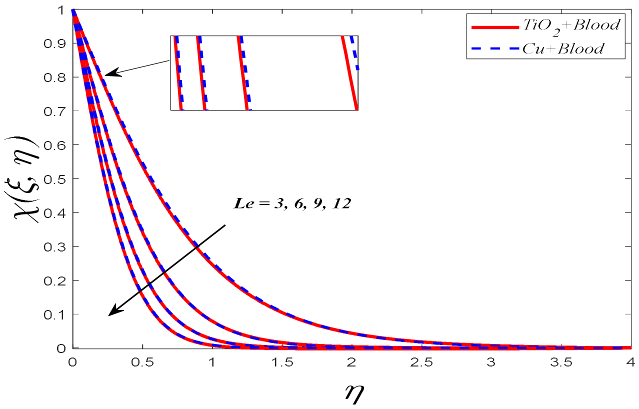

Figure 11. Variation of microorganism profile with different values of "Le".

If $\xi = 0.5, Q = 1.1, Ec = 1.8, Pr = 21, M = 0.25, \lambda = 1.5, F_r = 1.3, S_c = 2.8, K_r = 0.2, S_r = 0.1, Le = 0.7, \delta_1 = 0.3$.

Table 1 depicts the thermophysical characteristics of the nanofluid.

Table 1. The thermophysical characteristics of the nanofluid [25].

Property	Symbol	Defined
Viscosity	μ_{nf}	$\mu_{nf} = \frac{\mu_f}{(1-\phi)^{2.5}}$
Density	ρ_{nf}	$\rho_{nf} = (1-\phi)\rho_f + \phi\rho_s$
Heat Capacitance	$(\rho C_p)_{nf}$	$(\rho C_p)_{nf} = (1-\phi)\left(\rho C_p\right)_f + \phi(\rho C_p)_s$
Electric conductivity	σ_{nf}	$\sigma_{nf} = \left\{1 + \frac{3\left(\frac{\sigma_s}{\sigma_f} - 1\right)\phi}{\left(\frac{\sigma_s}{\sigma_f} + 2\right) - \left(\frac{\sigma_s}{\sigma_f} - 1\right)\phi}\right\}\sigma_f$
Thermal Conductivity	k_{nf}	$k_{nf} = \frac{\left(k_s + 2k_f\right) - 2\phi(k_f - k_s)}{\left(k_s + 2k_f\right) + \phi(k_f - k_s)} k_f$
Mass Diffusivity	D_{nf}	$D_{nf} = (1-\phi)D_f$

Table 2 presents the thermophysical properties of both base fluids and nanoparticles.

Table 2. The thermophysical characteristics of nanoparticles in conjunction with the base fluid.

Physical property	Blood	ZnO	TiO_2
$\rho(m^{-3}Kg)$	1063	5700	4250
$C_p(K^{-1}JKg^{-1})$	3594	523	686.2
$k(K^{-1}Wm^{-1})$	0.492	25	8.9538
$\sigma(\Omega.m^{-1})$	0.8	2×10^{-6}	1.0×10^{-12}

Tables 3 and **4** present a discussion on the Nusselt number and drag force coefficient responses for different parameter values.

Table 3 shows the direct relation of different parameters with $Re^{\frac{1}{2}}C_f$, as the parameters M, λ, and F_r increase, the value of $Re^{\frac{1}{2}}C_f$ also increase.

Table 3. Calculated the $-Re^{\frac{1}{2}}C_f$ values for different M, λ, and F_r predictions, assuming ξ=0.5, and $Pr = 21$.

M	λ	F_r	ZnO + Blood	TiO_2 + Blood
0.2	0.5	0.6	0.43782910	0.40347623
0.4	0.5	0.6	0.43871489	0.40448743
0.6	0.5	0.6	0.43946105	0.40452139
0.8	0.5	0.6	0.44163052	0.40453278
0.25	1	0.6	0.01638520	0.06201482
0.25	3	0.6	0.02561956	0.06321946
0.25	5	0.6	0.02581405	0.06422105

Table 3. (*Continued*).

M	λ	F_r	ZnO + Blood	TiO_2 + Blood
0.25	7	0.6	0.02816391	0.07249543
0.25	0.5	0.5	0.13734056	0.27510531
0.25	0.5	1.0	0.14246190	0.27621021
0.25	0.5	1.5	0.14349561	0.29218945
0.25	0.5	2.0	0.15302185	0.29317220

Table 4 shows the inverse relation of different parameters with $Re^{\frac{1}{2}}Nu$, as the parameters M, λ, Ec, and Q increase, the value of $Re^{\frac{1}{2}}Nu$ decrease.

Table 4. Calculated the $-Re^{\frac{1}{2}}Nu$ values for $M, \lambda, Ec,$ and Q predictions, assuming ξ=0.5, and $Pr = 21$.

M	λ	Ec	Q	ZnO + Blood	TiO_2 + Blood
0.2	0.5	0.2	0.4	0.71026721	0.62393745
0.4	0.5	0.2	0.4	0.70827642	0.62137012
0.6	0.5	0.2	0.4	0.70472011	0.61274624
0.8	0.5	0.2	0.4	0.69321064	0.59387251
0.25	1	0.2	0.4	0.39174290	0.33865102
0.25	3	0.2	0.4	0.37812301	0.33682306
0.25	5	0.2	0.4	0.37520173	0.31852047
0.25	7	0.2	0.4	0.34193084	0.31638561
0.25	0.5	0.4	0.4	0.51030618	0.48261823
0.25	0.5	0.8	0.4	0.50593821	0.47726582
0.25	0.5	1.2	0.4	0.50262145	0.45451894
0.25	0.5	1.6	0.4	0.48923073	0.44327632
0.25	0.5	0.2	0.3	0.03914723	0.29526081
0.25	0.5	0.2	0.5	0.01736814	0.29418652
0.25	0.5	0.2	0.7	0.01519354	0.27862091
0.25	0.5	0.2	0.9	0.01284067	0.27127912

Table 5 illustrates a comparison between our study and the works done by El. Aziz [35], Loganathan and Vimla [36], and Sharma [37].

Table 5. Comparison of $-\theta'(0)$ across various values of Pr, in a scenario where Q, Ec, M and λ are all equal to zero, and ξ is set to 0.5.

Pr	El. Aziz [35]	Loganathan and Vimla [36]	Sharma [37]	Present Study
1	0.954785	0.955870	0.954788	0.955271
3	1.869074	1.868878	1.869073	1.868219
5	2.500132	2.499982	2.500121	2.522403
10	3.660372	3.660239	3.660289	3.661172

5. Conclusion

In the problem being examined, a non-similar analysis of MHD boundary layer flow with Darcy-Forchheimer bioconvection of nanofluids is proposed in the study. The study has provided insights into the impact of the nanoparticles TiO_2 and ZnO on the flow dynamics and transport phenomena within the boundary layer. Further investigations may be warranted to explore the long-term effects and potential applications of utilizing TiO_2 and ZnO in nanofluid systems, particularly in the context of medical treatments and therapies. Understanding the behavior of these particles within MHD boundary layer flows is crucial for optimizing their utilization and ensuring their safe and effective implementation in various fields. The study investigates the impact of relevant parameters on velocity, temperature, nanoparticles volume fraction, and microorganism distribution within appropriate ranges. To tackle the highly nonlinear governing system, a combination of the LNS technique and the MATLAB bvp4c (built-in package) is employed successfully. This study's findings can be summed up as follows:

- The velocity profile collapses with the higher magnetic field (M), porosity (λ), and Forchheimer number (F_r) parameters.
- By enhancing the magnetic field, porosity, and Eckert number parameters, the temperature profile improved.
- The concentration profile is reduced when the Schmidt number (Sc) is increased but improved when the Soret number (Sr) is increased.
- The microorganism's profile reduced as the Lewis number (Le) grew, whereas it increased as the Peclet number (Pe) increased.
- Increases in the magnetic field, porosity, and Forchheimer number lead to an rise in the drag coefficient.
- The local Nusselt number decreases as the magnetic field, porosity, Eckert number, and heat source increase.
- A comparative study has been conducted to bolster the current research, showcasing the coherence of the current findings.
- Future endeavors may focus on the refinement of medical imaging modalities such as magnetic resonance imaging (MRI), the optimization of radiation therapy methodologies for cancer treatment, and the incorporation of perspectives from heat transfer studies on stretched surfaces into biomedical device development, to improve both safety and effectiveness in medical era.

Author contributions: Conceptualization, methodology, software, writing, UF (Umar Farooq); supervision and project administration, TL; formal analysis, review and editing, data curation, UF (Umer Farooq). All authors have read and agreed to the published version of the manuscript.

Acknowledgments: This work was supported in part by the NSFC Grant No. 52175033 and No. U21A20120; the Key Research and Development Program of Zhejiang under awards 2022C03103 and 2021C03051. Umar Farooq, Tao Liu are with the State Key Laboratory of Fluid Power & Mechatronic Systems, School of Mechanical Engineering, Zhejiang University, 310027, Hangzhou.

Conflict of interest: The authors declare no conflict of interest.

References

1. Buongiorno J, Hu LW. Nanofluid Heat Transfer Enhancement for Nuclear Reactor Applications. Available online: https://dspace.mit.edu/handle/1721.1/65899 (accessed on 17 March 2024).
2. Buongiorno J. Convective Transport in Nanofluids. Journal of Heat Transfer. 2005; 128(3): 240-250. doi: 10.1115/1.2150834
3. Duangthongsuk W, Wongwises S. Effect of thermophysical properties models on the predicting of the convective heat transfer coefficient for low concentration nanofluid. International Communications in Heat and Mass Transfer. 2008; 35(10): 1320-1326. doi: 10.1016/j.icheatmasstransfer.2008.07.015
4. Khan MWS, Ali N. Thermal entry flow of power-law fluid through ducts with homogeneous slippery wall(s) in the presence of viscous dissipation. International Communications in Heat and Mass Transfer. 2021; 120: 105041. doi: 10.1016/j.icheatmasstransfer.2020.105041
5. Ali N, Khan MWS, Saleem S. Critical analysis of generalized Newtonian fluid flow past a non-linearly stretched curved surface: A numerical solution for Carreau model. ZAMM - Journal of Applied Mathematics and Mechanics / Zeitschrift für Angewandte Mathematik und Mechanik. 2023; 104(2). doi: 10.1002/zamm.202300100
6. Mehmood Y, Shafqat R, Sarris IE, et al. Numerical Investigation of MWCNT and SWCNT Fluid Flow along with the Activation Energy Effects over Quartic Auto Catalytic Endothermic and Exothermic Chemical Reactions. Mathematics. 2022; 10(24): 4636. doi: 10.3390/math10244636
7. Kandasamy R, Loganathan P, Arasu PP. Scaling group transformation for MHD boundary-layer flow of a nanofluid past a vertical stretching surface in the presence of suction/injection. Nuclear Engineering and Design. 2012; 241(6): 2053-2059. doi: 10.10115/2012/934964
8. Crane LJ. Flow past a stretching plate. Zeitschrift für angewandte Mathematik und Physik ZAMP. 1970; 21(4): 645-647. doi: 10.1007/bf01587695
9. Yazdi MH, Abdullah S, Hashim I, et al. Slip MHD liquid flow and heat transfer over non-linear permeable stretching surface with chemical reaction. International Journal of Heat and Mass Transfer. 2011; 54(15-16): 3214-3225. doi: 10.1016/j.ijheatmasstransfer.2011.04.009
10. Farooq U, Hussain M, Farooq U. Non-similar analysis of chemically reactive bioconvective Casson nanofluid flow over an inclined stretching surface. ZAMM - Journal of Applied Mathematics and Mechanics/Zeitschrift für Angewandte Mathematik und Mechanik. 2023; 104(2). doi: 10.1002/zamm.202300128
11. Abuasbeh K, Shafqat R, Niazi AUK, et al. Mild Solutions for the Time-Fractional Navier-Stokes Equations with MHD Effects. Symmetry. 2023; 15(2): 280. doi: 10.3390/sym15020280
12. Magyari E, Keller B. Heat and mass transfer in the boundary layers on an exponentially stretching continuous surface. Journal of Physics D: Applied Physics. 1999; 32(5): 577-585. doi: 10.1088/0022-3727/32/5/012
13. Darcy H. Les Fontaines publiques de la ville de Dijon; Exposition et application des principes à suivre et des formules à employer dans les questions de distribution d'eau ... (French). Legare Street Press; 2022.
14. Forchheimer PH. Water movement through soil (German). Available online: https://cir.nii.ac.jp/crid/1572261549273889536 (accessed on 16 March 2024).
15. Wang J, Mustafa Z, Siddique I, et al. Computational Analysis for Bioconvection of Microorganisms in Prandtl Nanofluid Darcy–Forchheimer Flow across an Inclined Sheet. Nanomaterials. 2022; 12(11): 1791. doi: 10.3390/nano12111791
16. Hady FM, Mohamed RA, Mahdy A, et al. Non-Darcy Natural Convection Boundary Layer Flow Over a Vertical Cone in Porous Media Saturated with a Nanofluid Containing Gyrotactic Microorganisms with a Convective Boundary Condition. Journal of Nanofluids. 2016; 5(5): 765-773. doi: 10.1166/jon.2016.1256.
17. Akbar, Y., Alotaibi, H., Iqbal, J., Nisar, K. S., & Alharbi, K. A. M. (2022). Thermodynamic analysis for bioconvection peristaltic transport of nanofluid with gyrotactic motile microorganisms and Arrhenius activation energy. Case Studies in Thermal Engineering, 34, 102055.
18. Iqbal J, Abbasi FM, Nawaz R. Numerical investigation of magnetohydrodynamic bioconvection peristalsis of Powell–Eyring nanofluid. Numerical Heat Transfer, Part A: Applications. Published online March 2024: 1-22. doi: 10.1080/10407782.2024.2322102.

19. Farooq U, Liu T, Farooq U, et al. Non-similar analysis of bioconvection MHD micropolar nanofluid on a stretching sheet with the influences of Soret and Dufour effects. Applied Water Science. 2024; 14(6). doi: 10.1007/s13201-024-02143-0
20. Abbas A, Shafqat R, Jeelani MB, et al. Convective Heat and Mass Transfer in Third-Grade Fluid with Darcy–Forchheimer Relation in the Presence of Thermal-Diffusion and Diffusion-Thermo Effects over an Exponentially Inclined Stretching Sheet Surrounded by a Porous Medium: A CFD Study. Processes. 2022; 10(4): 776. doi: 10.3390/pr10040776
21. Farooq U, Liu T, Farooq U, et al. Heat transfer analysis of ternary hybrid Williamson nanofluids with gyrotactic microorganisms across stretching surfaces: Local non-similarity method. Numerical Heat Transfer, Part A: Applications. Published online April 15, 2024: 1-22. doi: 10.1080/10407782.2024.2341431
22. Saeed Khan MW, Ali N, Bég OA. Thermal entrance problem for blood flow inside an axisymmetric tube: The classical Graetz problem extended for Quemada's bio-rheological fluid with axial conduction. Proceedings of the Institution of Mechanical Engineers, Part H: Journal of Engineering in Medicine. 2022; 236(6): 848-859. doi: 10.1177/09544119221086479
23. Abbas A, Shafqat R, Jeelani MB, et al. Significance of Chemical Reaction and Lorentz Force on Third-Grade Fluid Flow and Heat Transfer with Darcy–Forchheimer Law over an Inclined Exponentially Stretching Sheet Embedded in a Porous Medium. Symmetry. 2022; 14(4): 779. doi: 10.3390/sym14040779
24. Khan MWS, Ali N. Theoretical analysis of thermal entrance problem for blood flow: An extension of classical Graetz problem for Casson fluid model using generalized orthogonality relations. International Communications in Heat and Mass Transfer. 2019; 109: 104314. doi: 10.1016/j.icheatmasstransfer.2019.104314
25. Farooq U, Farooq U. Non-similar analysis of bio-convective micropolar nanofluid flow including gyrotactic microorganisms across a stretched geometry. Numerical Heat Transfer, Part B: Fundamentals. 2024: 1-18. doi: 10.1080/10407790.2024.2333022
26. Khan MWS, Ali N. Thermal entry flow problem for Giesekus fluid inside an axis-symmetric tube through isothermal wall condition: a comparative numerical study between exact and approximate solution. Zeitschrift für Naturforschung A. 2021; 76(11): 973-984. doi: 10.1515/zna-2021-0098
27. Kuznetsov AV. Nanofluid bioconvection in water-based suspensions containing nanoparticles and oxytactic microorganisms: oscillatory instability. Nanoscale Research Letters. 2011; 6(1). doi: 10.1186/1556-276x-6-100
28. Farooq U, Liu T. Non-similar analysis of MHD bioconvective nanofluid flow on a stretching surface with temperature-dependent viscosity. Numerical Heat Transfer, Part A: Applications. 2023; 1-17. doi: 10.1080/10407782.2023.2279249
29. Tiwari RK, Das MK. Heat transfer augmentation in a two-sided lid-driven differentially heated square cavity utilizing nanofluids. International Journal of Heat and Mass Transfer. 2007; 50(9-10): 2002-2018. doi: 10.1016/j.ijheatmasstransfer.2006.09.034
30. Sparrow EM, Yu HS. Local Non-Similarity Thermal Boundary-Layer Solutions. Journal of Heat Transfer. 1971; 93(4): 328-334. doi: 10.1115/1.3449827
31. Rehman MIU, Chen H, Hamid A, et al. Theoretical investigation of Darcy-Forchheimer flow of bioconvection Casson fluid in the presence of chemical reaction effect. Biomass Conversion and Biorefinery. Published online July 27, 2022. doi: 10.1007/s13399-022-03060-5
32. Puneeth V, Anandika R, Manjunatha S, et al. Implementation of modified Buongiorno's model for the investigation of chemically reacting rGO-Fe3O4-TiO2-H2O ternary nanofluid jet flow in the presence of bio-active mixers. Chemical Physics Letters. 2022; 786: 139194. doi: 10.1016/j.cplett.2021.139194
33. Salahuddin T, Khan M, Saeed T, et al. Induced MHD impact on exponentially varying viscosity of Williamson fluid flow with variable conductivity and diffusivity. Case Studies in Thermal Engineering. 2021; 25: 100895. doi: 10.1016/j.csite.2021.100895
34. Devi SU, Devi SA. Heat transfer enhancement of Cu-Al_2O_3/water hybrid nanofluid flow over a stretching sheet. Journal of the Nigerian Mathematical Society. 2017; 36(2): 419-433.
35. Abd El-Aziz M. Viscous dissipation effect on mixed convection flow of a micropolar fluid over an exponentially stretching sheet. Canadian Journal of Physics. 2009; 87(4): 359-368. doi: 10.1139/p09-047
36. Loganathan P, Vimala C. MHD Boundary Layer Flow of a Nanofluid Over an Exponentially Stretching Sheet in the Presence of Radiation. Heat Transfer—Asian Research. 2013; 43(4): 321-331. doi: 10.1002/htj.21077
37. Sharma S. MHD Boundary Layer Flow Past an Exponentially Stretching Sheet with Darcy-Forchheimer Flow of Nanofluids. Indian Journal Of Science And Technology. 2022; 15(33): 1594-1604. doi: 10.17485/ijst/v15i33.607